Shock Waves (2022) 32:363–371
https://doi.org/10.1007/s00193-022-01082-6

ORIGINAL ARTICLE

Can ozonolysis reactions influence detonations?

C. B. Reuter[1,2] · T. M. Ombrello[2] · S. G. Tuttle[1]

Received: 23 July 2021 / Revised: 8 April 2022 / Accepted: 12 April 2022 / Published online: 22 May 2022

Abstract
Additives such as ozone have been shown both experimentally and numerically to enhance detonation properties, but the effects of ozone on one of the most common fuels used in detonation engines, ethylene, have not been sufficiently investigated. In the present study, the impact of ozonolysis reactions between ethylene and ozone on detonations is numerically examined in detail. Specifically, a combined flow reactor and detonation simulation is performed with residence times within the flow reactor corresponding to timescales relevant to detonation engines. The simulations are carried out over a range of equivalence ratios, ethylene–methane fuel blends, temperatures, and pressures. The results show that ozone addition to ethylene–methane–air mixtures leads to the formation of multiple peaks in thermicity. In some cases, particularly for lean mixtures or high ozone concentrations, the first peak in thermicity caused by the consumption of ozone can surpass the second peak caused by high-temperature fuel oxidation. It is also found that the maximum pressure of ozonolysis-assisted detonations decreases and the induction length increases for higher residence times. Comparisons are made between ozonolysis reactions and parasitic combustion due to the tendency of each to raise the pre-shock temperature but decrease the post-shock pressure.

Keywords Detonation · Ozone · Induction length · Ozonolysis reactions · Ethylene

1 Introduction

Although the vast majority of combustion engines rely on deflagration, detonative propulsion systems such as pulse detonation engines (PDEs) and rotating detonation engines (RDEs) are capable of even higher theoretical efficiencies [1]. Because of this, research on both fundamental aspects [2,3] and applications [4–6] of detonation waves has accelerated over the past 20 years. While detonation waves are three-dimensional and unstable, perhaps their most important parameter is a simple length scale, the cell size, which is formed by the paths of the triple points in space [7]. The detonation cell size, λ, has been shown to correlate well with many properties of detonation waves. It has a linear relationship with the induction length, Δ_I, [8–10] (although the ratio λ/Δ_I tends to be dependent on the mixture) and the critical tube diameter, d_c, [7,11,12] (for which d_c/λ is typically 13 for fuel–air mixtures). Additionally, the cube of the cell size has been shown to scale with the critical initiation energy [7,8,13], and correlations have been made between the cell size and the deflagration-to-detonation transition (DDT) distance for certain mixtures [14].

Since detonation engines have a wider range of operability for smaller detonation cell sizes [12,15,16], parameters which can decrease the cell size are of great interest. Recently, Crane et al. [10] experimentally revealed that the addition of ozone (O_3) leads to a reduction in the cell size. Other studies [17–20] have shown that Δ_I likewise decreases with O_3 addition. The DDT distance can also be smaller with the addition of O_3 [21,22].

However, the introduction of O_3 in mixtures with unsaturated hydrocarbons such as ethylene (C_2H_4) leads to ozonolysis reactions [23–25]. C_2H_4 is one of the primary hydrocarbons used in small-scale detonation experiments [22,26–28] and in detonation engines [29–32], but only a few investigations have examined the detonation properties of mixtures containing both C_2H_4 and O_3. Wang et al. [22] performed C_2H_4–O_2–O_3 detonation experiments at reduced pressures ($p \leq 30$ kPa$\approx$0.3 atm) and found that a small amount of O_3 promoted the onset time of DDT, but that

Communicated by G. Ciccarelli.

✉ C. B. Reuter
christopher.reuter.ctr@nrl.navy.mil

[1] U.S. Naval Research Laboratory, Chemistry Division, 4555 Overlook Avenue SW, Washington, DC 20375, USA

[2] U.S. Air Force Research Laboratory, Aerospace Systems Directorate, Wright-Patterson AFB, OH 45433, USA

excessive O_3 delayed DDT. They attributed this phenomenon to ozonolysis reactions between C_2H_4 and O_3 but did not perform any detailed analysis. In a different study, Kumar et al. [20] numerically simulated the impact of O_3 addition on C_2H_4–air mixtures and determined that the induction length decreases with O_3 addition in all instances; however, they did not include ozonolysis reactions in their chemical kinetic model. Therefore, it is still not known to what extent ozonolysis reactions can modify detonation properties or how their effects can change with mixture composition, temperature, or pressure.

This investigation aims to clarify the impact of ozonolysis reactions between C_2H_4 and O_3 on detonations. One-dimensional numerical simulations of detonation wave structure based on the Zel'dovich–von Neumann–Döring (ZND) model are performed for ethylene–methane–air mixtures with various levels of ozone addition. Due to its importance in determining the extent of ozonolysis reactions, the residence time prior to the detonation wave is considered for ranges that are relevant for PDEs and RDEs. The effects of different ethylene/methane ratios, equivalence ratios, pressures, and temperatures are also examined.

2 Simulation

The numerical simulations in this study are performed with a combination of Cantera 2.4.0 [33] and the Caltech Shock and Detonation Toolbox [34]. Specifically, the output from a FlowReactor module in Cantera is fed into a ZND computation in the Shock and Detonation Toolbox, which is similar to the approach of Romano et al. [35] in which a heated fuel–air mixture was allowed to undergo low-temperature oxidation before transitioning to a detonation. The flow reactor calculation is solved with an adiabatic boundary condition, an absolute tolerance of 10^{-15}, a relative tolerance of 10^{-9}, and a maximum timestep of 10^{-5} s. The residence time within the flow reactor (t_{res}), representing the time prior to the detonation wave, varies from 1 to 100 ms. Although PDEs can operate with frequencies between 1 and 100 Hz, t_{res} more directly corresponds to the sum of the fill and spark delay times, which is usually in the range of 15–40 ms [32,36,37]. RDEs have much higher frequencies of 1–10 kHz [5,15]; however, some RDEs run in a premixed mode, which can have extended residence times within the plenum [30]. The ZND calculation is performed with an absolute tolerance of 10^{-8}, a relative tolerance of 10^{-5}, and a maximum timestep of 10^{-4} s.

The chemical kinetic model (FFCM-ozonolysis) is identical to the one used in previous studies of ozonolysis-assisted combustion [38,39] and consists of a combination of the Foundational Fuel Chemistry Model version 1.0 (FFCM-1) [40] for the base hydrocarbon chemistry, HP-Mech [41] for the ozone chemistry, and four reactions from Rousso et al. [24] for describing ozonolysis between C_2H_4 and O_3. Specifically, the four reactions are the following:

$$C_2H_4 + O_3 = CH_2O + CO + H_2O \quad (1)$$

$$C_2H_4 + O_3 = CH_2O + CO_2 + H_2 \quad (2)$$

$$C_2H_4 + O_3 = CH_2O + CO_2 + H + H \quad (3)$$

$$C_2H_4 + O_3 = CH_2O + HCO + OH. \quad (4)$$

Since most commercial ozone generators require pure O_2 to produce O_3, the ozone concentration is defined as the mole fraction of O_3 in the O_2–O_3 mixture. Ozone concentrations of up to 3% O_3 are examined in this study, which correspond to O_3 mole fractions of 5600–6000 ppm in the overall C_2H_4–CH_4–N_2–O_2–O_3 mixture, depending on the equivalence ratio and fuel blending. The equivalence ratio (ϕ) considers both O_2 and O_3 in determining the fuel/oxidizer ratio, specifically, $\phi = (3X_{C2H4} + 2X_{CH4})/(X_{O2} + 1.5X_{O3})$. The ethylene content refers to the mole fraction of C_2H_4 in the C_2H_4–CH_4 fuel mixture. The N/O ratio is fixed at 3.762 so that a mixture with 0% O_3 addition is "air." Finally, Δ_I is defined as the distance (x) from the shock wave (at $x = 0$) to the location of the maximum thermicity.

3 Results and discussion

3.1 Effects of ozonolysis on detonation structure

The impact of O_3 addition on C_2H_4–CH_4–air detonations is first examined without the upstream flow reactor computation ($t_{res} = 0$ ms), i.e., only including the ZND computation. The initial (pre-shock) conditions are $p = 1$ atm (101.3 kPa) and $T = 300$ K. Figure 1 shows that O_3 addition results in a local maximum in the thermicity (σ), an increase in the peak σ, and a decrease in Δ_I. The local maximum in the spatial profile of σ becomes more pronounced with higher levels of O_3 addition. With 3% O_3 addition, for example, the first peak in σ near $x = 0.014$ mm is more than half of the second peak near $x = 0.76$ mm.

Figure 2 shows the spatial profiles of temperature, pressure, thermicity, and mole fraction for the 3% O_3 case. The consumption of O_3, as shown by the blue line in Fig. 2b, is partially responsible for the local peak in σ near $x = 0.014$. Specifically, the reactions most contributing to the first peak in thermicity are $H + O_3 = O_2 + OH$, $C_2H_3 + O_2 = CH_2O + HCO$, and $HCO + O_2 = CO + HO_2$. The main peak in σ near $x = 0.76$ mm is caused by the oxidation of even smaller intermediate species by reaction pathways typically associated with high-temperature combustion chemistry such as $CH_3 + O = CH_2O + H$, $H_2 + OH = H + H_2O$, $H + O_2 + M = HO_2 + M$, and $HCO + OH = CO + H_2O$.

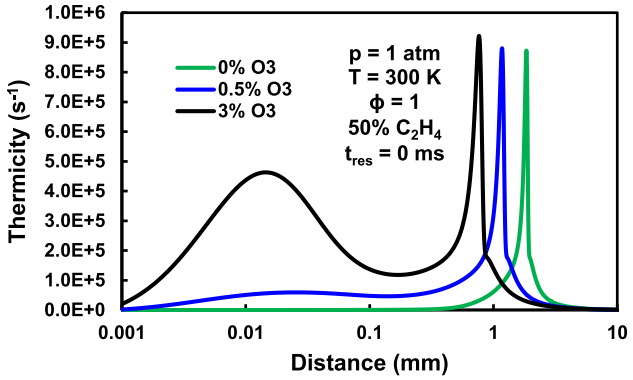

Fig. 1 Computed spatial profiles of thermicity for stoichiometric 50% C_2H_4–50% CH_4–air detonations with three different levels of O_3 addition

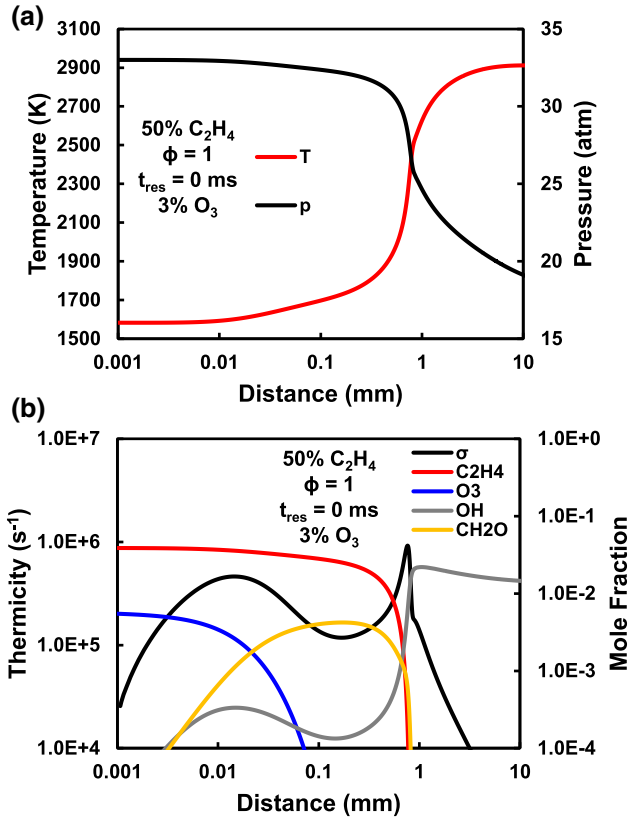

Fig. 2 Spatial profiles of **a** temperature and pressure and **b** thermicity and mole fraction for a 50% C_2H_4–50% CH_4–air detonation with 3% O_3 addition

3.2 Effects of residence time

When a flow reactor simulation is performed prior to the ZND computation, ozonolysis reactions produce a rise in temperature, even under atmospheric pressure ($p = 1$ atm = 101.3 kPa) and room temperature ($T = 300$ K) conditions. The temperature rise at the end of the flow reactor (T_{end}) increases for longer t_{res} and higher O_3 concentrations

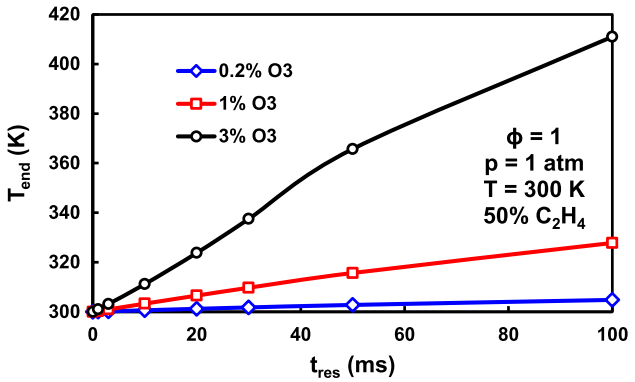

Fig. 3 Temperature at the end of the flow reactor as a function of residence time for three different levels of O_3 addition in 50% C_2H_4–50% CH_4–air mixtures

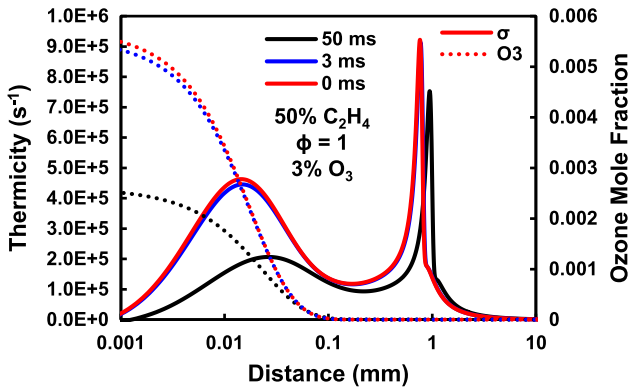

Fig. 4 Spatial profiles of thermicity and O_3 mole fraction for 50% C_2H_4–50% CH_4–air detonations with 3% O_3 addition at three different flow reactor residence times

(Fig. 3). At the highest T_{end} of 411 K occurring with 3% O_3 addition, 90% and 11% of the initial O_3 and C_2H_4 are consumed, respectively. The amount of O_3 and C_2H_4 consumed, moreover, is directly proportional to T_{end} for a given O_3 concentration, confirming that the pre-shock temperature rise is primarily due to ozonolysis reactions ($\sim$ 70% of the overall heat release rate).

Figure 4 shows the differences in the spatial profiles of σ and O_3 mole fraction for three different t_{res}. The $t_{res} = 0$ ms and $t_{res} = 3$ ms cases have nearly the same Δ_I and maximum σ since less than 3% of the initial O_3 is consumed in the flow reactor for the $t_{res} = 3$ ms case. However, for the $t_{res} = 50$ ms case, the post-shock O_3 mole fraction is only 45% of that of the $t_{res} = 0$ ms case. As a result, the local maximum in σ is reduced significantly (below even that of the 0% O_3 case), and Δ_I is 24% larger than that of the $t_{res} = 0$ ms case. Therefore, for cases with higher t_{res}, the extended time for ozonolysis reactions to proceed results in a smaller amount of post-shock O_3 in the mixture, which leads to a reduction in both peaks in σ and a longer Δ_I for the detonation, despite the rise in pre-shock temperature (Fig. 3).

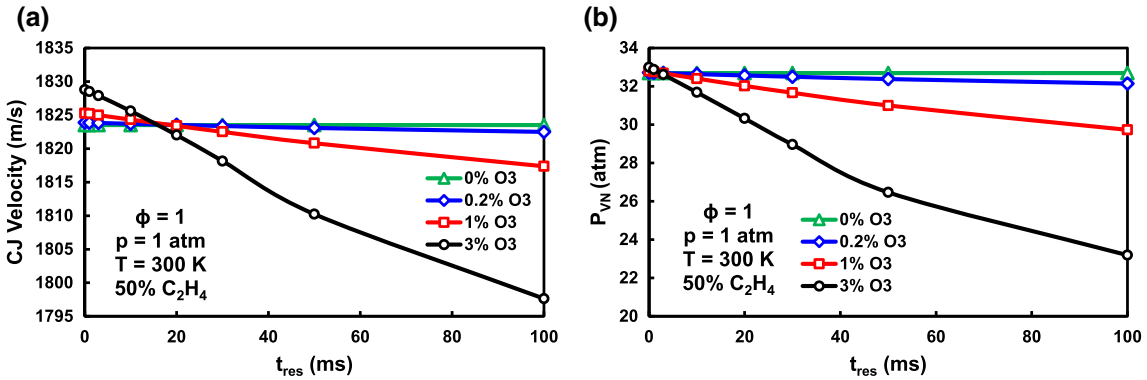

Fig. 5 Decreases in **a** Chapman–Jouguet velocity and **b** pressure at the von Neumann state with increasing flow reactor residence time for four different levels of O_3 addition in 50% C_2H_4–50% CH_4–air detonations

Other effects of extended t_{res} are shown in Fig. 5. The Chapman–Jouguet velocity (U_{CJ}) slightly rises with O_3 addition at short t_{res} (Fig. 5a); for example, the addition of 3% O_3 produces an increase of 5 m/s in U_{CJ} at $t_{res} = 0$ ms. However, U_{CJ} decreases more substantially for long t_{res}, as the same addition of 3% O_3 results in a drop of more than 13 m/s at $t_{res} = 50$ ms. The crossover point at which O_3 addition negatively impacts U_{CJ} is approximately at $t_{res} = 15$ ms for all O_3 concentrations examined. Similarly, the pressure at the von Neumann state (p_{VN}) marginally increases from $p = 32.7$ atm with 0% O_3 to $p = 33.0$ atm with 3% O_3 at $t_{res} = 0$ ms (Fig. 5b); however, at $t_{res} = 50$ ms, 3% O_3 produces a 19% decrease in p_{VN}. Moreover, the crossover point for p_{VN} occurs much earlier (~ 3 ms). The weakened detonation at high O_3 concentration and long t_{res} is reminiscent of "parasitic combustion" or "preburning" that can occur in detonation engines [42–45]. In both cases, subsonic fuel consumption leads to a pre-shock temperature rise, and the detonation that follows has a reduced wave speed and peak pressure. Additionally, since the interaction between shocks and flames can be an important precursor to DDT [46], the reduction in p_{VN} as ozonolysis reactions progress (Fig. 5b) may also possibly explain the results of Wang et al. [22], in which excess O_3 addition delayed the DDT process in C_2H_4–O_2–O_3 mixtures.

Figure 6 reveals the impact of t_{res} on Δ_I. Unlike U_{CJ} and p_{VN}, Δ_I is monotonically dependent on O_3 concentration for all t_{res} (i.e., there is no crossover point). Another difference is that the relationship between Δ_I and O_3 addition is highly nonlinear, even at short t_{res}. A small amount of O_3 can produce a large change in Δ_I. For example, the addition of 0.2% O_3 leads to an almost 30% reduction in Δ_I; in contrast, 0.2% O_3 addition changes p_{VN} by 1–2% at most. However, O_3 addition is also less effective on Δ_I at long t_{res}, particularly for higher O_3 concentrations. As shown in Fig. 7, 3% O_3 addition goes from decreasing Δ_I by 59% at $t_{res} = 0$ ms to 49% at $t_{res} = 50$ ms. At $t_{res} = 100$ ms, in fact,

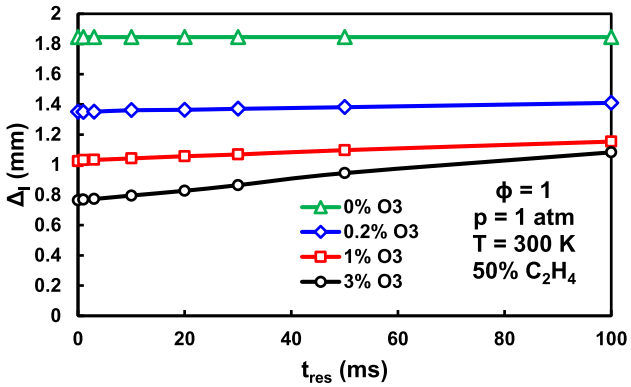

Fig. 6 ZND induction length as a function of flow reactor residence time for four different levels of O_3 addition in 50% C_2H_4–50% CH_4–air detonations

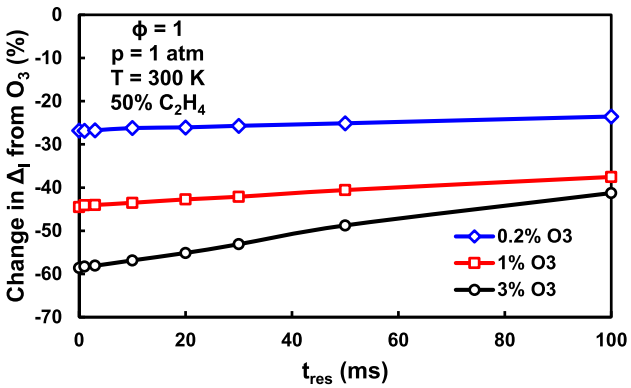

Fig. 7 Relative change in induction length with O_3 addition as a function of flow reactor residence time for 50% C_2H_4–50% CH_4–air detonations

3% O_3 addition is only slightly more impactful than 1% O_3 addition. Overall, the effects of ozonolysis reactions on detonation properties at extended t_{res} are complicated—while p_{VN} is considerably lower compared to that of the detonation without O_3 addition (indicative of a weaker detonation), Δ_I is much shorter (indicative of a stronger detonation).

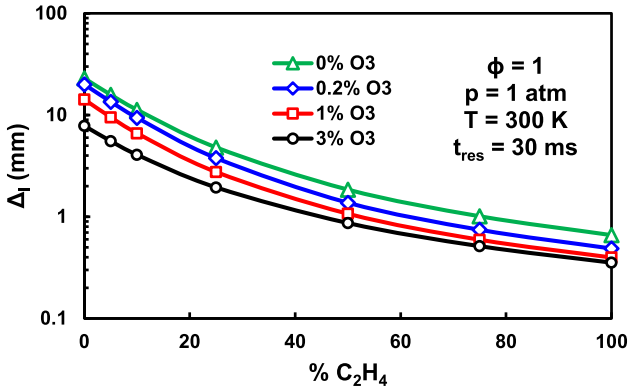

Fig. 8 ZND induction length as a function of ethylene content for four different levels of O_3 addition at a residence time of 30 ms

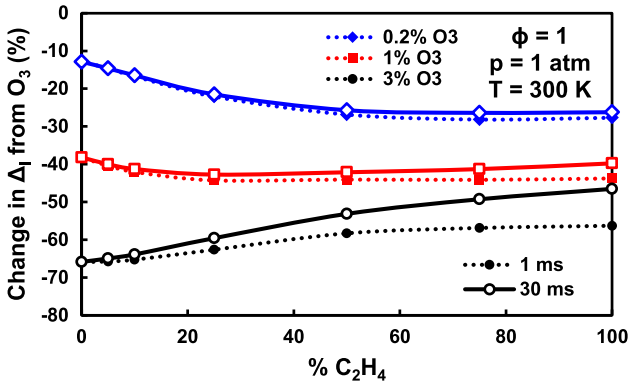

Fig. 9 Relative change in induction length with O_3 addition as a function of ethylene content for residence times of 1 ms (dotted lines) and 30 ms (solid lines)

3.3 Effects of changes in ethylene content

In order to examine the interplay between O_3 addition and fuel reactivity on detonation structure, Fig. 8 displays Δ_I as a function of ethylene content at $t_{res} = 30$ ms. It is clear that Δ_I is quite sensitive to the C_2H_4/CH_4 ratio. Without O_3 addition, a 0% C_2H_4 mixture (i.e., 100% CH_4) has a Δ_I more than 30 times larger than that of a 100% C_2H_4 mixture, which is why methane–air mixtures have rarely been successfully used in detonation engines [6]. At $t_{res} = 30$ ms, however, increasing amounts of O_3 result in decreasing Δ_I across all levels of ethylene content. For example, the 50% C_2H_4 case with 1% O_3 addition ($\Delta_I = 1.07$) has nearly the same Δ_I as the 75% C_2H_4 case without O_3 addition ($\Delta_I = 1.01$).

The change in Δ_I with O_3 addition for different levels of ethylene content is shown in Fig. 9. For both residence times ($t_{res} = 1$ ms and 30 ms), the relationship between ethylene content and the change in Δ_I is modified by the amount of O_3 addition. Specifically, the 0.2% O_3 cases display larger relative decreases in Δ_I with increasing ethylene content, but the 3% O_3 cases have the opposite trend. The impact of ozonolysis reactions also becomes clearer at higher amounts of O_3 addition. While there is not much difference between the $t_{res} = 1$ ms and $t_{res} = 30$ ms cases at 0.2% O_3, a distinct separation is apparent at 3% O_3. At 100% C_2H_4, in fact, the difference between the two residence times at 3% O_3 is 10% (i.e., a 46% decrease in Δ_I versus a 56% decrease). Note that t_{res} has no influence on Δ_I for the 0% C_2H_4 case since ozonolysis reactions do not occur for pure methane.

3.4 Effects of changes in equivalence ratio

When O_3 is added to a mixture at lean equivalence ratios, it is possible for the first peak in σ to exceed the second peak in σ. Figure 10 reveals an example of such an occurrence. At $t_{res} = 30$ ms, the second peak in σ at $x = 4.44$ mm is slightly lower than the first peak in σ at $x = 0.032$ mm for

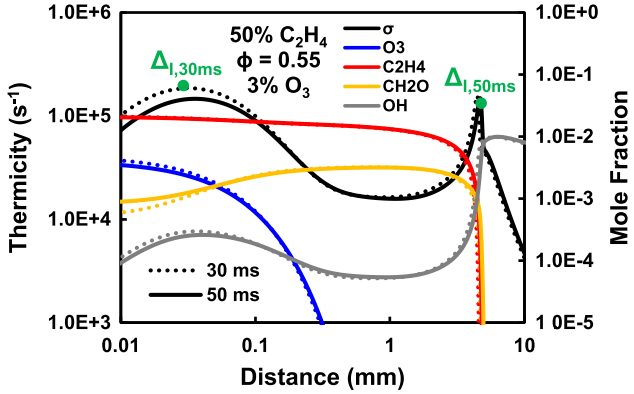

Fig. 10 Spatial profiles of thermicity and mole fraction with 3% O_3 addition at residence times of 30 ms (dotted lines) and 50 ms (solid lines) for 50% C_2H_4–50% CH_4–air detonations

the $\phi = 0.55$ mixture with 3% O_3; therefore, Δ_I is shorter by approximately two orders of magnitude compared to the same case with $t_{res} = 50$ ms in which $\Delta_I = 4.69$ mm. For ozone-assisted detonations, however, it is unclear whether parameters such as the critical ignition energy or the critical tube diameter would scale with this first peak in σ within the ozone decomposition zone, as implied by Kumar et al. [20] for mixtures with large amounts of O_3 addition. For example, the authors in [20] computed that $\Delta_I = 0.010$ mm (which is within the ozone decomposition zone) for their stoichiometric C_2H_4–air case with 15,000 ppm O_3, but the second peak in σ for this condition is at $x \approx 0.180$ mm in the middle of the high-temperature reaction zone. As has been stated previously by Ng et al. [47], experimental measurements are needed in the future to determine how detonation properties (e.g., critical tube diameter) scale for detonations with multiple peaks in thermicity.

Figure 11 shows Δ_I as a function of t_{res} for four different equivalence ratios. Note that the second peak in Δ_I of the $\phi = 0.55$ case is also included for reference. Even with 3% O_3, Δ_I is still strongly dependent on the equivalence

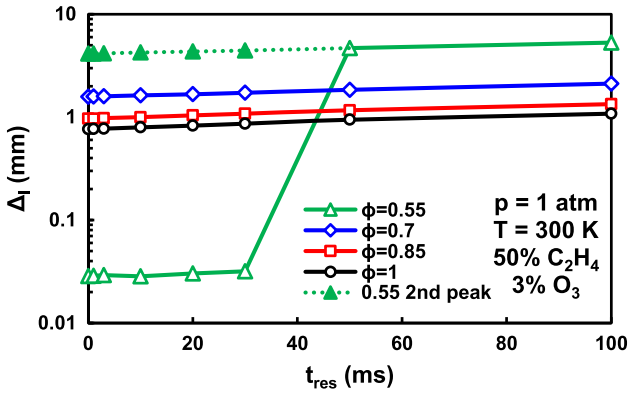

Fig. 11 ZND induction length with 3% O_3 addition as a function of flow reaction residence times for four different equivalence ratios in 50% C_2H_4–50% CH_4–air detonations

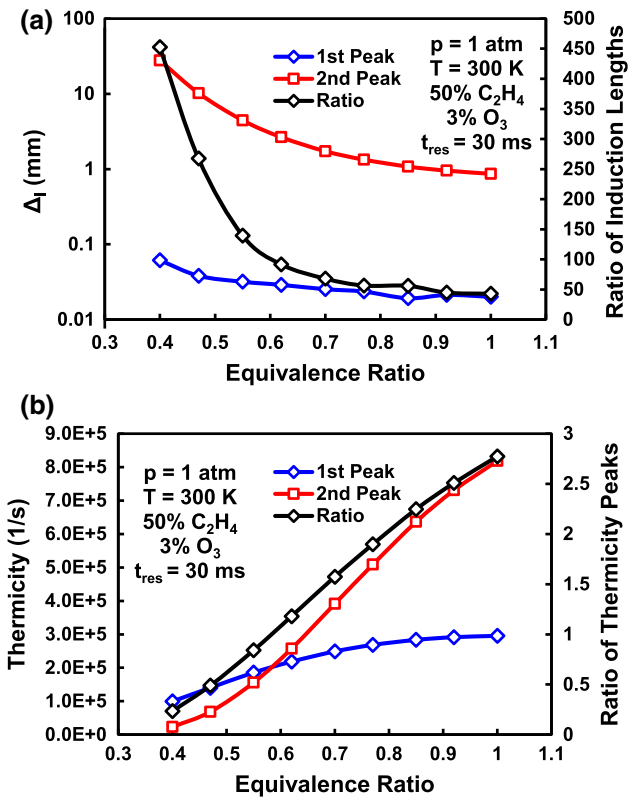

Fig. 12 Calculated **a** first and second peaks in induction length and **b** first and second peaks in thermicity in 50% C_2H_4–50% CH_4–air detonations with 3% O_3 addition

ratio. For example, at $t_{res} \leq 30$ ms, $\Delta_I = 1.0$–1.1 mm for the $\phi = 0.85$ case and 4.2–4.4 mm for the $\phi = 0.55$ case. The effect of increased t_{res} is also slightly lower at decreased equivalence ratios, shifting from a 24% difference in Δ_I between the $t_{res} = 0$ ms and $t_{res} = 50$ ms cases at $\phi = 1$ to a 17% difference over the same range at $\phi = 0.7$. The reduced consumption of O_3 in the lean case (39% at $\phi = 0.7$ versus 55% at $\phi = 1$) is thought to be responsible for this discrepancy. Therefore, for a given t_{res}, the progress of ozonolysis reactions impacts the detonation structure to a slightly lesser degree at lower equivalence ratios.

The occurrence of detonations with two-step heat release has been investigated previously for nitromethane-O_2 [48], H_2–NO_2 [49], and dimethyl ether-O_2 mixtures [47], which can result in experimental observation of "double cellular detonations" under certain conditions [50]. Likewise, detonations with two peaks in thermicity for C_2H_4–CH_4–air mixtures with O_3 addition are shown in Fig. 12. The first and second induction lengths (Fig. 12a) tend to decrease with increasing ϕ, and the first and second peaks in thermicity (Fig. 12b) monotonically increase with increasing ϕ. As seen previously in Fig. 11, the first peak in thermicity surpasses the second peak in thermicity for very lean ($\phi > 0.6$) equivalence ratios. This unusual characteristic (most of the previous studies observed two peaks in thermicity in rich mixtures [48], and none had a crossover point in the maximum thermicity) is due to the simple fact that there is more O_3 relative to fuel for leaner mixtures. In other words, O_3 consumption increases as fuel oxidation weakens. Additionally, the ratio between the first and second peaks in thermicity ranges from 2.8 at $\phi = 1$ to 0.23 at $\phi = 0.4$, which is a wide variation compared to other mixtures [51]. The ratio between the first and second induction lengths, likewise, spans approximately an order of magnitude from 43 to 450. Of course, these ratios are significantly modified when either t_{res} or the O_3 concentration changes.

The relative change in Δ_I from 3% O_3 addition is shown in Fig. 13 for both the 50% C_2H_4 case and the 100% C_2H_4 case. For both fuel blends, the relative decrease in Δ_I is more prominent for lower equivalence ratios; additionally, the impact of ozonolysis reactions (i.e., the sensitivity to t_{res}) at a given equivalence ratio is similar between the two blends. Interestingly, the 50% C_2H_4 case has a larger relative decrease in Δ_I than the 100% C_2H_4 case for $\phi = 1$ and $\phi = 0.85$ but a smaller decrease for $\phi = 0.55$. This trend is consistent across the entire range of t_{res} examined. It should be noted, however, that for 0.2% O_3 addition (not shown) the relative decrease in Δ_I is greater for the 100% C_2H_4 case across all lean equivalence ratios, which is not altogether surprising considering the trends from Fig. 9.

3.5 Effects of changes in pressure and temperature

Since the wall temperatures in detonation engines can reach 800 K or higher over the span of a few seconds [5,52], the temperature of the fresh gas mixture can be modified by heat transfer from the walls. Figure 14a shows Δ_I for initial temperatures of 300 K, 400 K, and 500 K. With 0% O_3 addition, Δ_I is a strict function of temperature; for example, Δ_I of the $T = 500$ K case is $\sim$ 30% smaller than that of the

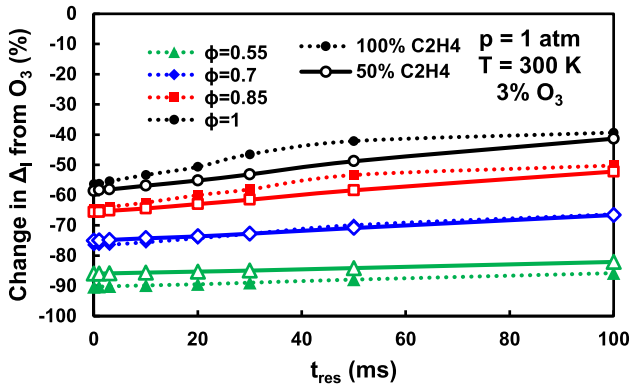

Fig. 13 Relative change in induction length with O_3 addition for four different equivalence ratios at 100% C_2H_4 (dotted lines) and 50% C_2H_4 (solid lines)

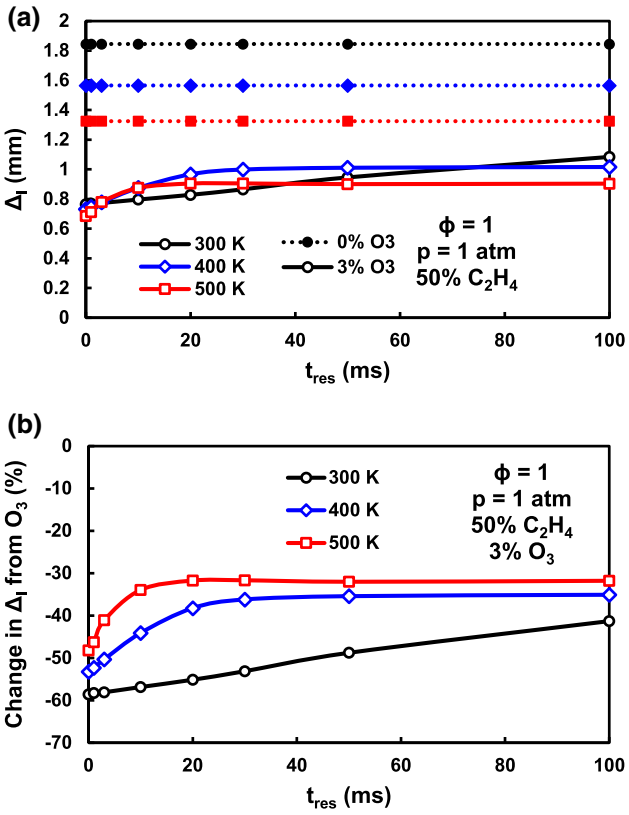

Fig. 14 Calculated **a** ZND induction length and **b** relative change in induction length with 3% O_3 addition as a function of flow reactor residence time for three different temperatures in 50% C_2H_4–50% CH_4–air detonations

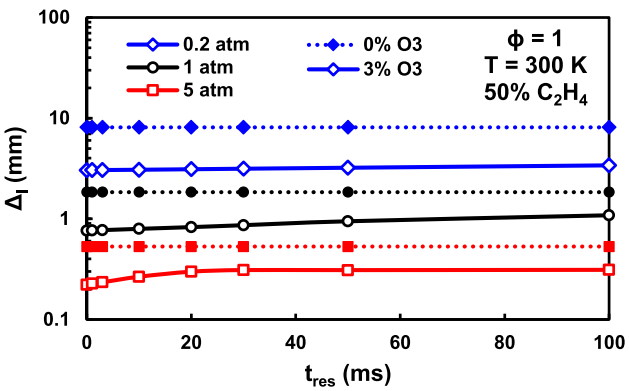

Fig. 15 ZND induction length as a function of flow reactor residence time for three different pressures with 0% O_3 addition (dotted lines) and 3% O_3 addition (solid lines) in 50% C_2H_4–50% CH_4–air detonations

$T = 300$ K case. However, with 3% O_3 addition, higher temperatures result in faster ozonolysis reaction rates for a given t_{res}, which leads to some interesting trends in Δ_I. At $t_{res} = 0$ ms, Δ_I of the $T = 500$ K case ($\Delta_I = 0.69$ mm) is slightly smaller than those of the $T = 400$ K ($\Delta_I = 0.73$ mm) and $T = 300$ K ($\Delta_I = 0.76$ mm) cases. At moderate residence times such as $t_{res} = 20$ ms, the order becomes jumbled ($\Delta_{I,300\,K} < \Delta_{I,500\,K} < \Delta_{I,400\,K}$). Finally, at $t_{res} = 100$ ms, at which point almost all of the O_3 is consumed before the shock, Δ_I regains the original trend ($\Delta_{I,500\,K} < \Delta_{I,400K} < \Delta_{I,300\,K}$).

The relative change in Δ_I, as shown in Fig. 14b, is consistently less pronounced for higher temperatures. For $T = 300$ K, the decrease in Δ_I is nearly linear with t_{res} due the progress of ozonolysis reactions. However, the trend for $T = 500$ K case is much less linear as a result of the increased ozonolysis reaction rates at higher temperatures; in fact, the decrease in Δ_I plateaus at 32% for $t_{res} \geq 20$ ms due to all of the O_3 being consumed. This, of course, is due to the changes in pre-shock O_3 consumption with temperature. Specifically, at $t_{res} = 20$ ms in Fig. 14, 20%, 82%, and 99% of O_3 have been consumed prior to the shock for $T = 300$ K, 400 K, and 500 K, respectively. Ozonolysis reactions consume 71%, 76%, and 71% of this pre-shock O_3, respectively. Therefore, increasing the temperature is not the most effective way to reduce Δ_I for ozonolysis-assisted detonations because the effects of higher post-shock temperatures and increased ozonolysis reaction rates tend to cancel each other out. Additionally, the pressure gain (i.e., p_{VN}) is higher at $T = 300$ K than at $T = 500$ K, which offsets the higher initial temperature.

Finally, although changes in temperature have only moderate effects on Δ_I with O_3 addition, modifying the pressure still considerably impacts Δ_I. Figure 15 displays how Δ_I decreases with increasing pressure for both 0% O_3 and 3% O_3 addition. Depending on the pressure, the relationship between Δ_I and t_{res} can be nearly constant ($p = 0.2$ atm = 20.3 kPa), linear ($p = 1$ atm = 101.3 kPa), or nonlinear ($p = 5$ atm = 506.6 kPa) with O_3 addition. For the lowest pressure case of $p = 0.2$ atm, only 22% of the initial O_3 is consumed before the shock for $t_{res} = 100$ ms. Moreover, as previously seen in the higher-temperature cases, higher pressures of $p = 5$ atm result in increased

ozonolysis reaction rates and the nearly complete ($\sim$ 98%) consumption of O_3 by $t_{res} = 30$ ms. Additionally, the relative decrease in Δ_I (not shown) of the $p = 5$ atm case is extremely similar for $t_{res} = 0$ ms ($\sim$ 59%) and $t_{res} = 100$ ms ($\sim$ 41%) to the $p = 1$ atm case but less pronounced at moderate t_{res}.

4 Conclusions

The answer to the question posed in the title of this paper is a mild "yes." While ozonolysis reactions are unlikely to affect the general sizing requirements of a detonation engine, they can cause similar effects to parasitic combustion. In particular, for residence times relevant to pulse detonation engines (15–40 ms), this investigation revealed that ozonolysis reactions had appreciable effects on the detonation properties of ethylene–methane–air mixtures with ozone addition. Ozone addition resulted in larger peak pressures, higher maximum thermicities, and shorter induction lengths for short residence times. However, at extended residence times, the detonation weakened due to the consumption of ethylene by ozonolysis reactions. Higher ozone concentrations led to more extreme deviations in the peak pressure.

Ozone addition also had a tremendous effect on the induction length. The largest relative decreases in the induction length occurred for shorter residence times, higher ozone concentrations, leaner mixtures, and lower temperatures. For very lean mixtures or high ozone concentrations, the peak in thermicity in the ozone consumption zone exceeded the peak in thermicity caused by high-temperature fuel oxidation. At extended residence times, ozonolysis reactions resulted in longer induction lengths, especially for elevated pressure and temperature conditions. However, the ozonolysis-affected induction lengths still had values well below those without ozone addition.

Acknowledgements This research was performed while C. B. Reuter held a National Research Council (NRC) Research Associateship Award at the Air Force Research Laboratory and an American Society for Engineering Education (ASEE) Postdoctoral Fellowship Award at the Naval Research Laboratory.

Data availability Data sharing is not applicable to this article as no datasets were generated or analyzed during the current study.

References

1. Wolanski, P.: Detonative propulsion. Proc. Combust. Inst. **34**, 125–158 (2013). https://doi.org/10.1016/j.proci.2012.10.005
2. Lee, J.H.S.: The Detonation Phenomenon. Cambridge University Press, Cambridge (2018). https://doi.org/10.1017/CBO9781316226926
3. Shepherd, J.E.: Detonation in gases. Proc. Combust. Inst. **32**, 83–98 (2009). https://doi.org/10.1016/j.proci.2008.08.006
4. Kailasanath, K.: Recent developments in the research on pulse detonation engines. AIAA J. **41**, 145–159 (2003). https://doi.org/10.2514/2.1933
5. Lu, F.K., Braun, E.M.: Rotating detonation wave propulsion: experimental challenges, modeling, and engine concepts. J. Prop. Power **30**, 1125–1142 (2014). https://doi.org/10.2514/1.B34802
6. Anand, V., Gutmark, E.: Rotating detonation combustors and their similarities to rocket instabilities. Prog. Energy Combust. Sci. **73**, 182–234 (2019). https://doi.org/10.1016/j.pecs.2019.04.001
7. Lee, J.H.S.: Dynamic parameters of gaseous detonations. Annu. Rev. Fluid Mech. **16**, 311–336 (1984). https://doi.org/10.1146/annurev.fl.16.010184.001523
8. Westbrook, C.K.: Chemical kinetics of hydrocarbon oxidation in gaseous detonations. Combust. Flame **46**, 191–210 (1982). https://doi.org/10.1016/0010-2180(82)90015-3
9. Gavrikov, A.I., Efimenko, A.A., Dorofeev, S.B.: A model for detonation cell size prediction from chemical kinetics. Combust. Flame **120**, 19–33 (2000). https://doi.org/10.1016/S0010-2180(99)00076-0
10. Crane, J., Shi, X., Singh, A.V., Tao, Y., Wang, H.: Isolating the effect of induction length on detonation structure: hydrogen–oxygen detonation promoted by ozone. Combust. Flame **200**, 44–52 (2019). https://doi.org/10.1016/j.combustflame.2018.11.008
11. Knystautas, R., Lee, J.H., Guirao, C.M.: The critical tube diameter for detonation failure in hydrocarbon-air mixtures. Combust. Flame **48**, 63–83 (1982). https://doi.org/10.1016/0010-2180(82)90116-X
12. Vasil'ev, A.A.: Cell size as the main geometric parameter of a multifront detonation wave. J. Propuls. Power **22**, 1245–1260 (2006). https://doi.org/10.2514/1.20348
13. Bull, D.C., Elsworth, J.E., Shuff, P.J., Metcalfe, E.: Detonation cell structures in fuel/air mixtures. Combust. Flame **45**, 7–22 (1982). https://doi.org/10.1016/0010-2180(82)90028-1
14. Dorofeev, S.B., Sidorov, V.P., Kuznetsov, M.S., Matsukov, I.D., Alekseev, V.I.: Effect of scale on the onset of detonations. Shock Waves **10**, 137–149 (2000). https://doi.org/10.1007/s001930050187
15. Roy, A., Bedick, C.R., Ferguson, D.H., Sidwell, T., Strakey, P.A.: Investigating instabilities in a rotating detonation combustor operating with natural gas-hydrogen fuel blend–effect of air preheat and annulus width. J. Eng. Gas Turbines Power **141**, 111017 (2019). https://doi.org/10.1115/1.4044980
16. Walters, I.V., Journell, C.L., Lemcherfi, A., Gejji, R.M., Heister, S.D., Slabaugh, C.D.: Operability of a natural gas-air rotating detonation engine. J. Propuls. Power **36**, 453–464 (2020). https://doi.org/10.2514/1.B37735
17. Magzumov, A.E., Kirillov, I.A., Rusanov, V.D.: Effect of small additives of ozone and hydrogen peroxide on the induction-zone length of hydrogen-air mixtures in a one-dimensional model of a detonation wave. Combust. Expl. Shock Waves **34**, 338–341 (1998). https://doi.org/10.1007/BF02672728
18. Mével, R., He, Y.Z.: Effect of oxygen atom precursors addition on LTC-affected detonation in DME–O_2–CO_2 mixtures. Shock Waves **30**, 799–807 (2020). https://doi.org/10.1007/s00193-020-00953-0
19. Crane, J., Shi, X., Xu, R., Wang, H.: Natural gas versus methane: Ignition kinetics and detonation limit behavior in small tubes. Combust. Flame. **237**, 111719 (2022). https://doi.org/10.1016/j.combustflame.2021.111719
20. Kumar, D.S., Ivin, K., Singh, A.V.: Sensitizing gaseous detonations for hydrogen/ethylene-air mixtures using ozone and H_2O_2 as dopants for application in rotating detonation engines. Proc. Combust. Inst. **38**, 3825–3834 (2021). https://doi.org/10.1016/j.proci.2020.08.061
21. Sepulveda, J., Rousso, A., Ha, H., Chen, T., Cheng, V., Kong, W., Ju, Y.: Kinetic enhancement of microchannel detonation transition

by ozone addition to acetylene mixtures. AIAA J. **57**, 476–481 (2019). https://doi.org/10.2514/1.J057773
22. Wang, C., Gu, G.T., Han, W.H., Cai, Y.: Role of O_3 addition in the deflagration-to-detonation transition of an ethylene–oxygen mixture in a macroscale tube. Shock Waves **30**, 781–787 (2020). https://doi.org/10.1007/s00193-020-00981-w
23. Bailey, P.S.: The reactions of ozone with organic compounds. Chem. Rev. **58**, 925–1010 (1958). https://doi.org/10.1021/cr50023a005
24. Rousso, A.C., Hansen, N., Jasper, A.W., Ju, Y.: Low-temperature oxidation of ethylene by ozone in a jet-stirred reactor. J. Phys. Chem. A **122**, 8674–8685 (2018). https://doi.org/10.1021/acs.jpca.8b06556
25. Sun, W., Gao, X., Wu, B., Ombrello, T.: The effect of ozone addition on combustion: kinetics and dynamics. Prog. Energy Combust. Sci. **73**, 1–25 (2019). https://doi.org/10.1016/j.pecs.2019.02.002
26. Hasson, A., Avinor, M., Burcat, A.: Transition from deflagration to detonation, spark ignition, and detonation characteristics of ethylene–oxygen mixtures in a tube. Combust. Flame **49**, 13–26 (1983). https://doi.org/10.1016/0010-2180(83)90147-5
27. Moen, I.O., Ward, S.A., Thibault, P.A., Lee, J.H., Knystautas, R., Dean, T., Westbrook, C.K.: The influence of diluents and inhibitors on detonations. Proc. Combust. Inst. **20**, 1717–1725 (1985). https://doi.org/10.1016/S0082-0784(85)80668-8
28. Auffret, Y., Desbordes, D., Presles, H.N.: Detonation structure of C_2H_4–O_2–Ar mixtures at elevated initial temperature. Shock Waves **9**, 107–111 (1999). https://doi.org/10.1007/s001930050145
29. Brophy, C.M., Hanson, R.K.: Fuel distribution effects on pulse detonation engine operation and performance. J. Propuls. Power **22**, 1155–1161 (2006). https://doi.org/10.2514/1.18713
30. Andrus, I.Q., Polanka, M.D., King, P.I., Schauer, F.R., Hoke, J.L.: Experimentation of premixed rotating detonation engine using variable slot feed plenum. J. Propuls. Power **33**, 1448–1458 (2017). https://doi.org/10.2514/1.B36261
31. Nakagami, S., Matsuoka, K., Kasahara, J., Kumazawa, Y., Fujii, J., Matsuo, A., Funaki, I.: Experimental visualization of the structure of rotating detonation waves in a disk-shaped combustor. J. Propuls. Power **33**, 80–88 (2017). https://doi.org/10.2514/1.B36084
32. Murray, A.P., Smith, T.L., Pittman, E.D., Liu, H., Crisp, E.M., Moore, J.D., Risha, G.A.: Frequency and spark timing effects on thrust for pulse detonation engine. J. Propuls. Power **37**, 242–251 (2021). https://doi.org/10.2514/1.B38049
33. Goodwin, D.G., Speth, R.L., Moffat, H.K., Weber, B.W.: Cantera: an object-oriented software toolkit for chemical kinetics, thermodynamics, and transport processes. http://www.cantera.org (2018). Accessed 25 Jan 2022
34. Browne, S., Ziegler, J., Shepherd, J.E.: Numerical solution methods for shock and detonation jump conditions. GALCIT Report FM2006.006 (2008)
35. Romano, M.P., Radulescu, M.I., Higgins, A.J., Lee, J.H.S., Pitz, W.J., Westbrook, C.K.: Sensitization of hydrocarbon–oxygen mixtures to detonation via cool-flame oxidation. Proc. Combust. Inst. **29**, 2833–2838 (2002). https://doi.org/10.1016/S1540-7489(02)80346-7
36. Tucker, K.C., King, P.I., Schauer, F.R.: Hydrocarbon fuel flash vaporization for pulsed detonation combustion. J. Propul. Power **24**, 788–796 (2008). https://doi.org/10.2514/1.28412
37. Stevens, C., King, P., Nagley, E., Schauer, F.: Fuel composition and coking analysis of endothermically heated hydrocarbon fuels for use in a pulsed detonation engine. 47th AIAA Aerospace Sciences Meeting, Orlando, FL, AIAA Paper 2009-501 (2009). https://doi.org/10.2514/6.2009-501
38. Reuter, C.B., Ombrello, T.M.: Flame enhancement of ethylene/methane mixtures by ozone addition. Proc. Combust. Inst. **38**, 2397–2407 (2021). https://doi.org/10.1016/j.proci.2020.06.122
39. Reuter, C.B., Ombrello, T.M.: Numerical simulations of ozone addition to strained flames. Combust. Sci. Technol. (2022). https://doi.org/10.1080/00102202.2021.1923703
40. Smith, G.P., Tao, Y., Wang, H.: Foundational fuel chemistry model version 1.0 (FFCM-1). http://nanoenergy.stanford.edu/ffcm1 (2016). Accessed 25 Jan 2022
41. Zhao, H., Yang, X., Ju, Y.: Kinetic studies of ozone assisted low temperature oxidation of dimethyl ether in a flow reactor using molecular-beam mass spectrometry. Combust. Flame **173**, 187–194 (2016). https://doi.org/10.1016/j.combustflame.2016.08.008
42. Schwer, D.A., Kailasanath, K.: Physics of heat-release in rotating detonation engines. 53rd AIAA Aerospace Sciences Meeting, Kissimmee, FL, AIAA Paper 2015-1602 (2015). https://doi.org/10.2514/6.2015-1602
43. Chacon, F., Gamba, M. Study of parasitic combustion in an optically accessible continuous wave rotating detonation engine. AIAA SciTech Forum, San Diego, CA, AIAA Paper 2019-0473. (2019). https://doi.org/10.2514/6.2019-0473
44. Prakash, S., Raman, V.: The effects of mixture preburning on detonation wave propagation. Proc. Combust. Inst. **38**, 3749–3758 (2021). https://doi.org/10.1016/j.proci.2020.06.005
45. Sato, T., Chacon, F., White, W., Raman, V., Gamba, M.: Mixing and detonation structure in a rotating detonation engine with an axial air inlet. Proc. Combust. Inst. **38**, 3769–3776 (2021). https://doi.org/10.1016/j.proci.2020.06.283
46. Khokhlov, A.M., Oran, E.S.: Numerical simulation of detonation initiation in a flame brush: the role of hot spots. Combust. Flame **119**, 400–416 (1999). https://doi.org/10.1016/S0010-2180(99)00058-9
47. Ng, H.D., Chao, J., Yatsufusa, T., Lee, J.H.: Measurement and chemical kinetic prediction of detonation sensitivity and cellular structure characteristics in dimethyl ether–oxygen mixtures. Fuel **88**, 124–131 (2009). https://doi.org/10.1016/j.fuel.2008.07.029
48. Presles, H.N., Desbordes, D., Guirard, M., Guerraud, C.: Gaseous nitromethane and nitromethane–oxygen mixtures: a new detonation structure. Shock Waves **6**, 111–114 (1996). https://doi.org/10.1007/BF02515194
49. Joubert, F., Desbordes, D., Presles, H.N.: Detonation cellular structure in NO_2/N_2O_4-fuel gaseous mixtures. Combust. Flame **152**, 482–495 (2008). https://doi.org/10.1016/j.combustflame.2007.11.005
50. Guilly, V., Khasainov, B., Presles, H.N., Desbordes, D.: Simulation numérique des détonations à double structure cellulaire. C. R. Méc. **334**, 679–685 (2006). https://doi.org/10.1016/j.crme.2006.05.002
51. Mével, R., Gallier, S.: Structure of detonation propagating in lean and rich dimethyl ether–oxygen mixtures. Shock Waves **28**, 955–966 (2018). https://doi.org/10.1007/s00193-018-0837-x
52. Ishihara, K., Nishimura, J., Goto, K., Nakagami, S., Matsuoka, K., Kasahara, J., Matsuo, A., Funaki, I., Moriai, H., Mukae, H., Yasuda, K., Nakata, D., Higashino, K.: Study on a long-time operation towards rotating detonation rocket engine flight demonstration. 55th AIAA Aerospace Sciences Meeting, Grapevine, TX, AIAA Paper 2017-1062 (2017). https://doi.org/10.2514/6.2017-1062